Nep J Environ Sci (2023), 11(2), 35-53
https://doi.org/10.3126/njes.v11i2.58152
ISSN 2350-8647 (Print) 2542-2901

Research Article

Landslide susceptibility mapping of the Main Boundary Thrust region in Mandre-Khursanibari section of Arghakhanchi and Palpa districts, Lumbini province of Nepal

Kabi Raj Paudyal*, Rupendra Maharjan
Central Department of Geology, Institute of Science and Technology, Tribhuvan University, Kirtipur, Kathmandu, Nepal
(Received: 23 August 2023; Revised: 30 December 2023; Accepted: 31 December 2023)

Abstract
The Mandre-Khursanibari section of Arghakhanchi and Palpa districts consists of numerous landslides, small to large. Prospecting weak geological sections like the location of the Main Boundary Thrust (MBT) and inherently weak lithological settings in addition to other factors are the main objectives of the present research. In this study, the results of the landslide susceptibility analysis using frequency ratios (FR) are assessed. The Mandre-Khursanibari segment was subjected to landslide detection using imagery (Google Earth) with a spatial resolution of 50 cm. The landslide inventory was used to construct training and testing data. Based on topographic, geological, and land-use maps, nine contributing variables were identified. The FR ratings were established using the contributing elements and training data. The map illustrating landslide risk was produced by integrating the influencing components that determined FR ratings. The ROC-AUC curve shows a validation rate of 82.2 % in the present model of LSI. The three most important elements in the occurrence of the landslide, out of the nine potential causes, are distance from the thrust (MBT), land use, and distance from the road. However, the role of adverse lithological setting is found to be a minor in many sections of this region. The MBT is one of the main causes of landslides in this area.

Keywords: Frequency ratio, landslide susceptibility, MBT, Mandre-Khursanibari, Lumbini province

Introduction
The Himalayas stand out as the planet's most ever-changing and delicate mountain range, marked by ongoing tectonic activity. Their instability primarily stems from the mountains' rocks having a naturally weak geological setting. The main potential sites of landslides in the Nepal Himalayas are dictated by adverse geological conditions like the presence of thrusts, faults, and adverse lithology in addition to other triggering factors like steep slope, concentrated precipitation, and seismic activity (Acharya & Paudyal, 2023; Paudyal & Maharjan, 2022; Paudyal et. al, 2022; Dhahal & Paudyal, 2022; Neupane & Paudyal, 2021; K.C. et al., 2018; Budha et al., 2016). Moreover, the weak geological setting is another strong factor causing the landslides in the hilly regions of Nepal (Neupane et. al, 2023). Building safer infrastructure, reducing natural hazards, and halting environmental deterioration in the Himalayas shall all become significantly simpler with a better understanding of the terrain's geology and the interaction of many triggering factors (Upreti, 2001). Nepal's hilly areas, with their rough landscapes, frequent earthquakes, and heavy rains, are vulnerable to various natural dangers. Landslides can harm the region's growth over time (Paudyal & Maharjan, 2022).

The geomorphic and tectonic history of the Nepal Himalayas is partly responsible for the abundance of deep and steep river valleys in Nepal. Earthquakes, particularly in seismically active areas like Nepal, might endanger the slope's stability in the long run (Taylor & Burns, 2005).

Mandre-Khursanibari, the research area, is situated near the border of Nepal's Arghakhanchi and Palpa districts (Fig. 1). Because of the area's dissected and rough topography, as well as the existence of the Main Boundary Thrust (MBT) makes the study area prone to landslides (Upreti & Dhital, 1996). This section consists of numerous landslides and finding the cause of such landslides is one of the major tasks of the present study. Finding the cause helps to select effective techniques to mitigate the landslides and reduce the risk of further land sliding in the region. The overall region under investigation is approximately 62 sq. km, with an altitude range of 336 m to as high as 1500 m.

The research area is bordered between $27^{0}51'46"$ N, $83^{0}9'31"$ E to 27048'56" N, $83^{0}16'11"$ E. Local routes linking to Mahendra Rajmarg can be used to reach the region. The Mandre-Khursanibari region is prone to several slope instability difficulties because of the steep slope, rough landscape, and weak rock state.

Materials and Methods
It is crucial to infer that landslide causative variables affect the geographical distribution of landslides and that future landslides will occur under conditions similar to those of prior landslides for landslide susceptibility mapping (Lee & Talib, 2005) (Fig. 2). This study will attempt to identify the areas susceptible to landslides using the Frequency Ratio (FR) method to explore the statistical relationship between parameters and landslides in GIS platform.

*Corresponding author: paudyalkabi1976@gmail.com

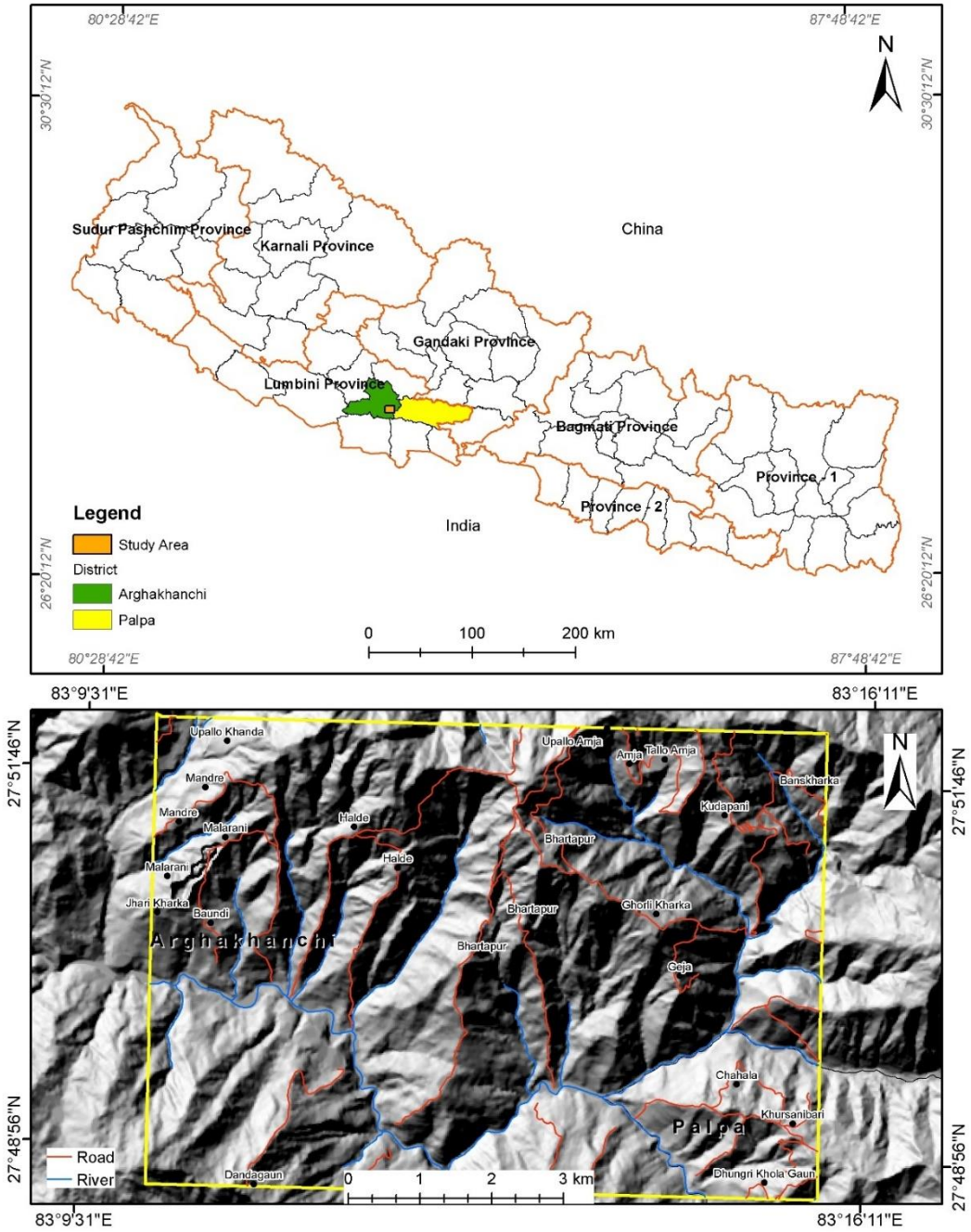

Figure 1 Location Map of Mandre-Khursanibari section.

Over the past few decades, numerous researchers have developed effective techniques for producing precise maps of landslide susceptibility. Frequency ratio (Goetz et al., 2015; Hong et al., 2016; Lee et al., 2017), logistic regression (Chen et al., 2017; Steger et al., 2016), decision trees (Lee & Park, 2013; Pradhan, 2013; Tsangaratos & Ilia, 2016), fuzzy logic (Feizizadeh et al., 2014; Park et al., 2014; Pradhan, 2011), neuro-fuzzy systems (Pradhan, 2013; Aghdam et al., 2016; Lee et al., 2015), support vector machines (Pradhan, 2013; Peng et al., 2014; Lee et al., 2017; Tien Bui et al., 2017), artificial neural networks (Conforti et al., 2014; Pradhan, 2011; Tsangaratos & Benardos, 2014), and multimethod approach (Althuwaynee et al., 2016; Pham et al., 2016; Pradhan, 2010; Yalcin et al., 2011) are a few approaches of these methods. The FR was utilized in the present investigation to assess the efficacy of the landslide susceptibility study.

The FR model has the advantage of ranking the causative variables in terms of their risk of producing a landslide and assessing whether a certain combination of causative factor values would be harmful in the event of a landslide (Kannan et al., 2013). Landslides

and debris flows are caused by the presence of numerous variables. During severe rains, when soil moisture levels are high and soil strength is low, shallow landslides are most likely to occur (Montgomery & Dietrich, 1994).

The landslide inventory of 72 was conducted using manual digitization of aerial photographs/satellite imagery from Google Earth (March-2020) and later verification field was carried out to assess the field reality of the region. The landslide inventory was afterward divided into training (70% - 50) and testing (30% - 22) samples. The landslide susceptibility index model (LSI) was developed using a training sample, and the model was validated using ROC-AUC in SPSS. Fig. 2 depicts the methodology used in the LSI mapping.

Thematic data layers must be prepared for landslide susceptibility mapping (Camarinha et al., 2014). As a result, nine thematic layers of 20 m × 20 m cell size were used: geology, slope, aspect, plan curvature, distance from the stream, distance from the thrust (MBT), distance from the road, relief, and land use land cover. To create topographic and hydrologic parameters, a digital elevation model (DEM) was prepared. For landslide susceptibility, topographic and hydrologic characteristics such as slope gradient, plan curvature, slope aspect, relief, and distance from the stream were taken into account. The satellite image was digitized in ArcMap10.4.1 to create the LULC map. The MBT and geology of the area have been obtained from the Department of Mines and Geology's geological map of the petroleum block 5. The Euclidean distance technique was used to calculate the distance to the MBT map.

After creating all nine rasters of influencing factors, a landslide inventory map was utilized to cross with the nine-factor maps to produce tabulated statistics which was used to carry out the FR method of landslide susceptibility mapping (LSI). The resulting LSI map was divided to stable, quasi-stable, unstable, and unstable zones.

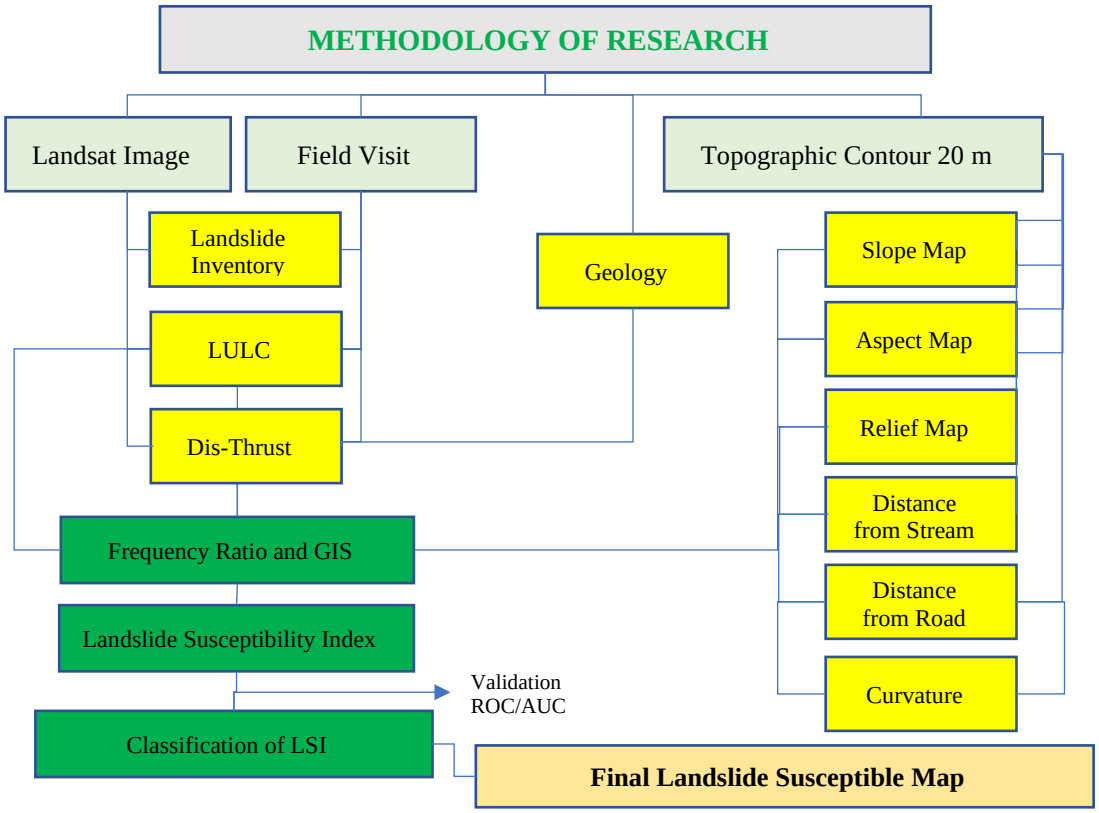

Figure 2 Methodology used in analysis of LSI mapping using FR method.

Frequency Ratio Method

It is necessary to understand the physical characteristics of the landscape as well as the mechanisms that cause landslides in order to determine the possibility of landslides. The frequency ratio is a quantitative method for measuring landslide risk that makes use of Geographic Information Systems (GIS) and geographical data (Bonham-Carter, 1994; Lee & Talib, 2005; Chen et al., 2016a; Chen et al., 2016b; Ding et al., 2017). The frequency ratio (FR) approach is widely and efficiently used for mapping landslide vulnerability (Yilmaz, 2009; Reis et al., 2012; Umar et al., 2014; Chen et al., 2016a; Wu et al., 2016; Wang & Li, 2017). It is based on the quantifiable relationship between the landslide inventories and the slide triggering variables (Reis et al., 2012). Using the Eq (1), a combination of

the landslide inventory map and the factor map was created to determine the frequency ratio (FR) for each class of the contributing components (Mondal & Maiti, 2013; Fayez et al., 2018).

$$Frequency\ Ratio\ (FR) = \frac{Npix\ (1)/Npix\ (2)}{\sum Npix\ (3)/\sum Npix\ (4)}$$ ----Eq. (1)

Where *Npix (1)* = The number of pixels containing Landslide in a class
Npix (2) = Total number of pixels of each class in whole area.
Npix (3) = Total number of pixels containing landslide.
Npix (4) = Total number of pixels in the study area.

Using Eq. (2), the calculated frequency ratio is aggregated to create a Landslide Susceptibility Index (LSI) map (Lee & Talib, 2005).

Landslide Susceptibility Index (LSI) = $FR_1 + FR_2 + FR_3 + FR_4 + \ldots\ldots\ldots + FR_n$ ---------- **Eq. (2)**

Results and Discussion

Landslide Inventory

Landslide inventory mapping is an essential aspect of landslide susceptibility mapping, which attempts to identify landslide-prone regions and the potential hazards they portray to people and infrastructure. Landslide inventory mapping entails collecting and analyzing data on historical and contemporary landslides in the targeted area. This information is used to assess the likelihood of future landslides and to develop effective strategies for mitigating the risks associated with them. 72 landslides with a total area of 0.243 km² were mapped using Landsat images that are accessible on Google Earth and fieldwork (Fig. 3).

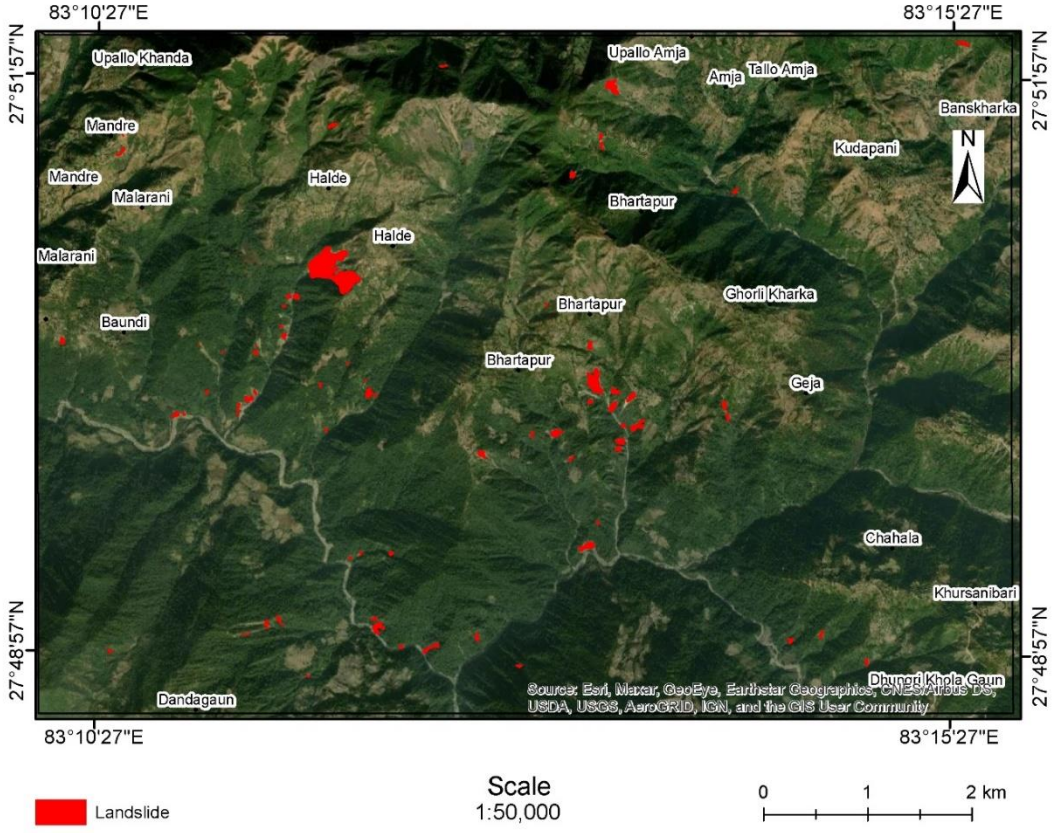

Figure 3 Landslide inventory map of the Mandre-Khursanibari area.

Influencing or Controlling Factors

Land-Use Land Cover

An image classification method was used to create a land cover map (Fig. 4). Table 1 shows that forest covers 72.5% of the entire area, agricultural land covers 20.1%, barren land covers 0.7%, and sand covers 1.2%. Crossing LULC data with current landslides reveals that forest area accounts for 49.2% of total landslide, barren land accounts for 42.5%, agricultural land accounts for 1.18%, and bushland accounts for 1.18% (Table 1). LULC serves as an important indicator for identifying landslide-prone areas (Ghimire, 2011).

With a high-frequency ratio of 62.48 compared to other classes like forests (0.68), shrubs (0.32), and (3.92), as well as agricultural land (0.09), which has the least FR, barren land is very prone to landslides by the frequency ratio for the land-use land cover (Table 2).

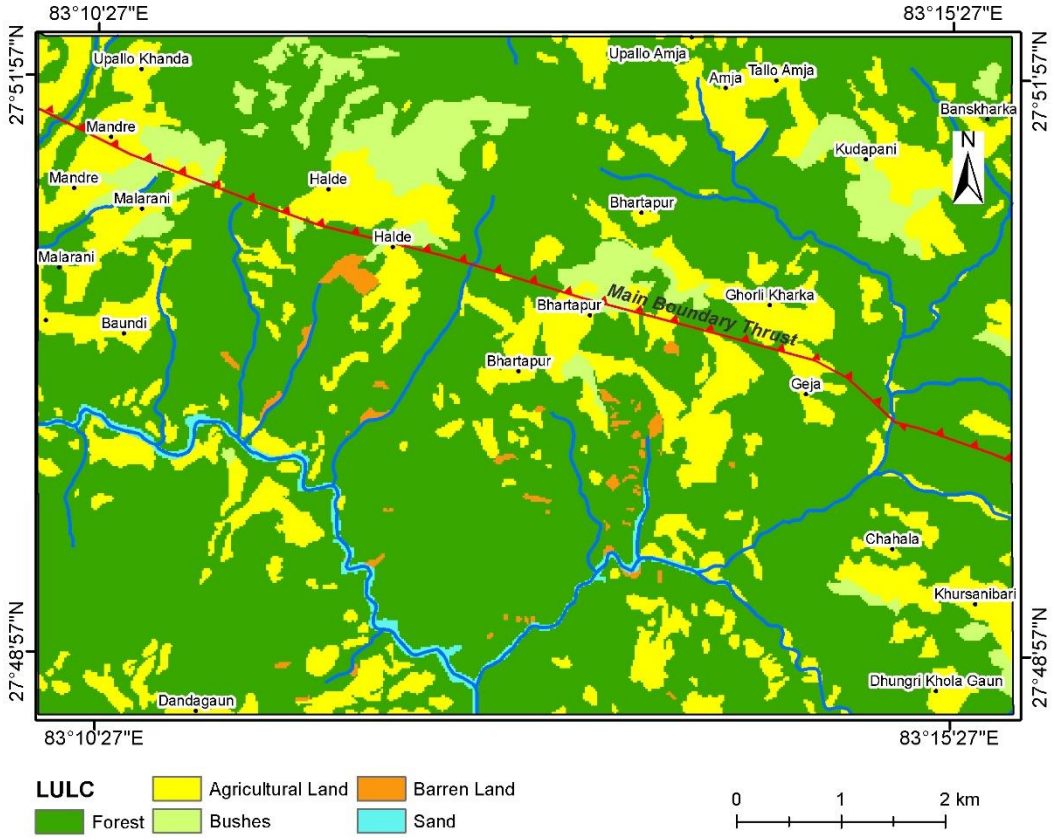

Figure 4 Land-use map of the study area.

Geology

For the landslide mapping, a geological map from the Department of Mines and Geology was adopted (Fig. 5). The research region is organized into eight primary lithological units based on its geology viz. the Lower Siwalik, Middle Siwalik, Swat Formation, Melpani Formation, Suntar Formation, Khara Formation, Katuwa Formation, Aru Formation, Charchare Formation, and the Gwar Formation. Table 1 demonstrates that the Middle Siwalik dominates the research region, making up 59.5% of the entire area, while 90.3% of the total landslides are present and have a FR of 1.52 at the same geology. The Aru Formation occupies an area of 11.4% and has a total of 5.6% of landslides. The Swat formation has FR value of 1.41 with 0.8% total area and 1.1% of the total landslide area. The Melpani Formation and the Suntar Formation, they only make up 3.1% and 1.1% of the entire study area, respectively, and there are no nearby landslides, they have the lowest frequency ratio of 0.

Distance to Thrust (MBT)

In this study, the distance to thrust (MBT) is an extrinsic parameter. The Main Boundary Thrust was located using the Geological map of exploration block number five by DMG-GON-1998. The block was then georeferenced, and the MBT's position was traced on the map. The MBT and Euclidean distance tool, which depicts each cell's link to a source or collection of sources based on the straight-line distance, were used to construct the distance to thrust map (Fig. 6). The five divisions of the map were spaced 500 m apart.

According to the study, 16.8% of all landslides happen within 0-500 m of the MBT, making this area the most prone to them. The highest Frequency Ratio (FR) figure in this zone, 2.41, supports this. Additionally, the number of landslides within 0.5 to 1 km from the MBT is significant (20.33%).

Slope

The slope map (Fig. 7) was created using the Surface-Spatial Analyst Tool in ArcMap and a 20*20 DEM (Digital Elevation Model). Using the equal interval classification approach, the slope is divided into six categories. According to Table 1, the slope angle range of 30^0 to 40^0 accounts for 39.68% of the research area and hosts 53% of all landslides. Similarly, slope angles between 10^0 and 20^0, 20^0 and 30^0, 40^0 and 50^0, and 50^0 and 64^0 respectively occupy 3.37%, 12.23%, 29.46%, 14.83%, and 0.43% of the total research area, while the corresponding slopes have landslides at rates of 3.1%, 6.6%, 22.8%, 14.1%, 0.8%, and 0.5%. According to Table 1, the terrain with slopes of 30^0–50^0 and 50^0–64^0 is most susceptible to landslides, with frequency ratios of 1.33 and 1.15, respectively, while the terrain with a slope gradient of 10^0–20^0 is least susceptible, with a frequency ratio of 0.09, likely due to the lower number of landslides that occur in that particular slope. Slope gradient and relative relief are identified as crucial

factors, and their calculated factor weight values correlate well with landslide susceptibility. This factor serves as proxy indicator for identifying landslide-prone areas (Ghimire, 2011).

Aspect Map

The Surface-Spatial Analyst Tool in ArcMap was used to create an aspect map for the research using a 20*20 DEM (Fig. 8). South-facing slopes, which made up 16.8% of the research area, were the predominant aspect among the eight groups of aspects (Table 1). Landslides were primarily seen on southeast-facing (20.49%), south-facing (19.34%), southwest-facing (18.69%), and west-facing (14.92%) sides. Aspect serves as an important indicator for identifying landslide-prone areas (Ghimire, 2011). The frequency ratio of the aspect map reveals that the southeast, south, southwest, and west aspects are are more prone to landslides, with the greatest frequency ratio values of 1.41, 1.15, 1.35, and 1.19, respectively (Table 1).

Relief Map

20*20 m DEM was used to create an elevation map, also known as a relief map, of the research region (Fig. 9). The greatest height is 1905 meters, while the lowest elevation is 336 meters. Four categories were used to categorize the relief map (Table 1). It was discovered that the elevation between 1000 and 1500 meters (m) accounts for 32.2% of the entire research area and contains 37.4% of all landslides, with a frequency ratio of 1.16.

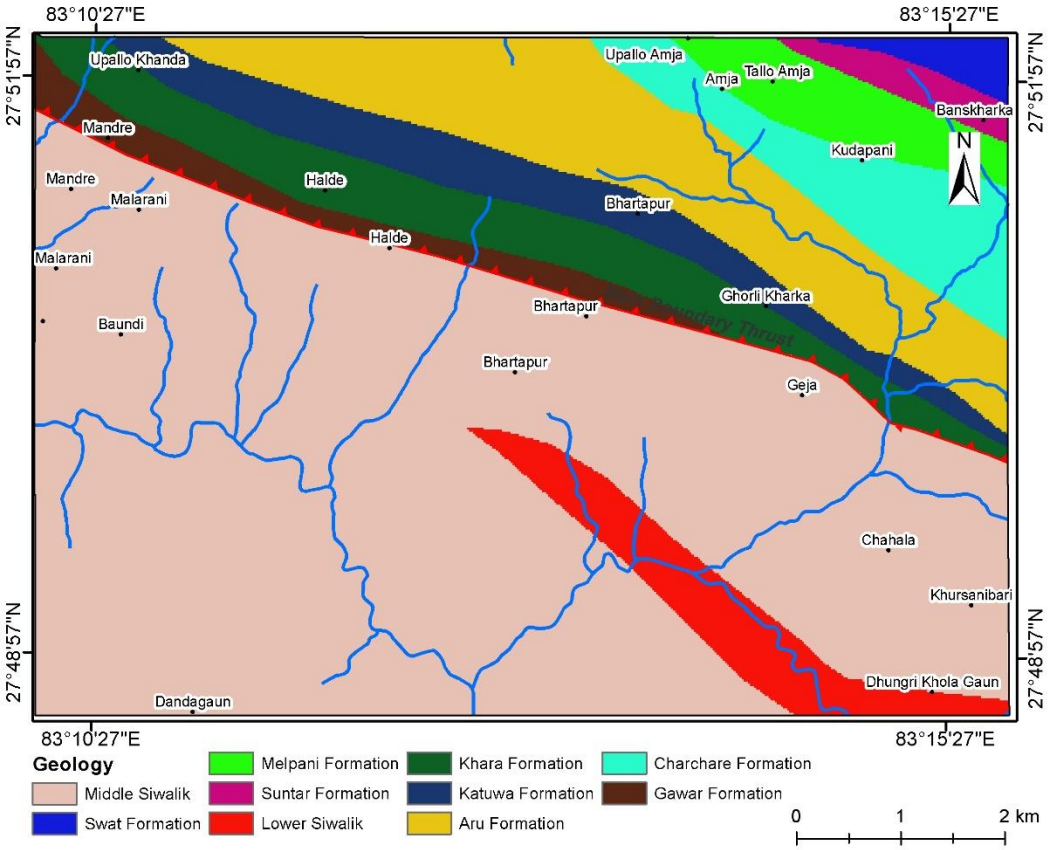

Figure 5 Geological map of the study area.

Distance from Stream

One of the key elements in determining landslide vulnerability is the stream. The distance to the stream map (Fig. 10) was created using the Euclidean distance tool, which represents each cell's relationship to a source or collection of sources based on the straight-line distance since the ground around the stream is more prone to landslides. There are five interval classes in it. According to Table 1, the region between 0 and 50 meters in diameter accounts for 12.0% of all landslides and 8.3% of the entire research area. Additionally, the region between 300 and 500 meters from the streams has a high-frequency ratio of 1.51 and is vulnerable to future landslides.

Curvature

The curvature, which is the departure of a surface from a plane or a curve from a straight line, is seen in Fig. 11. The curvature map was produced using a 20*20 m DEM and the Surface-Spatial Analyst Tool in ArcMap. The split of curvature into concave, linear, and convex surfaces is shown in Fig. 10. Table 1 shows that the studied region is more naturally convex than concave, with convex topography occupying 47.4% of the total area, concave topography covering 44.5% of the area, and linear or flat surface making up 8.1%.

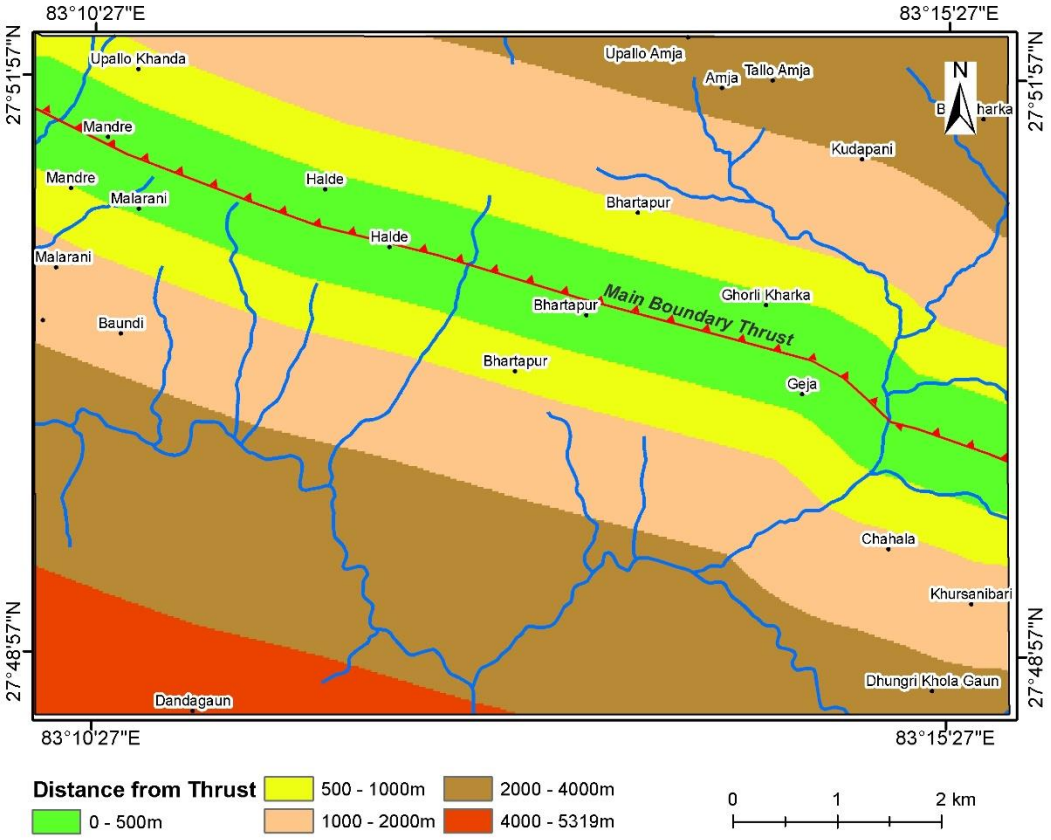

Figure 6 Distance from thrust map.

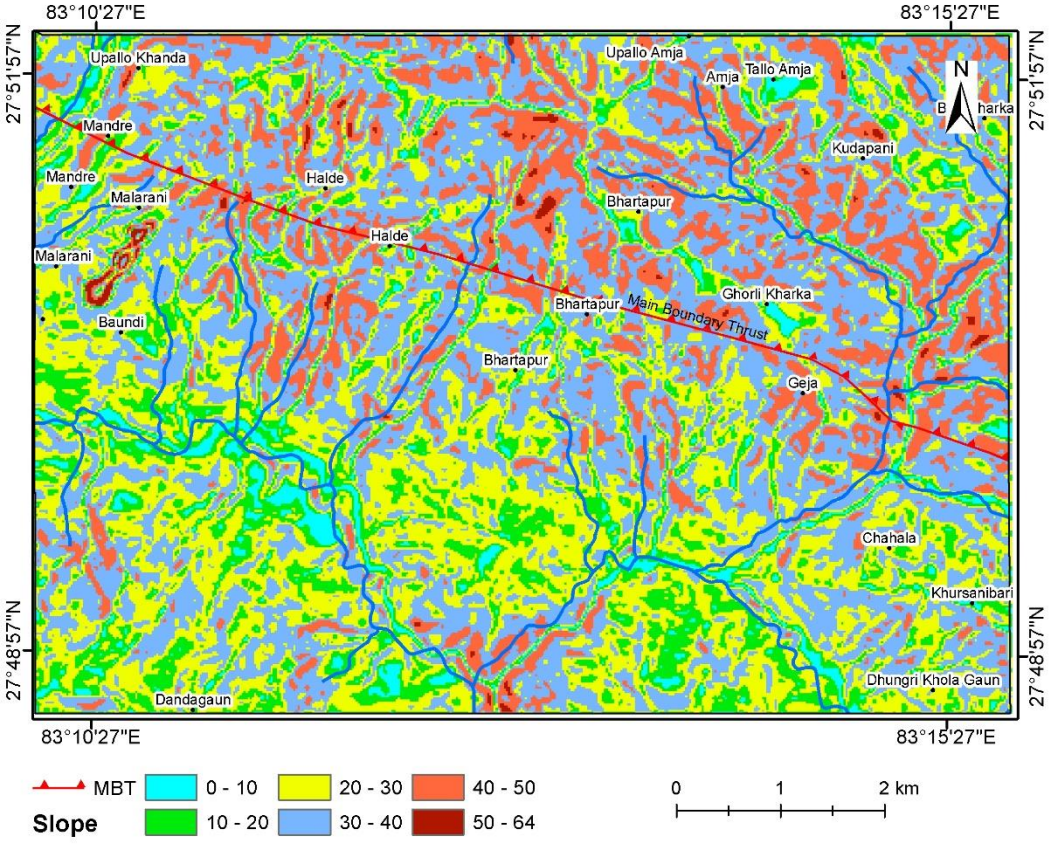

Figure 7 Slope map of the study area.

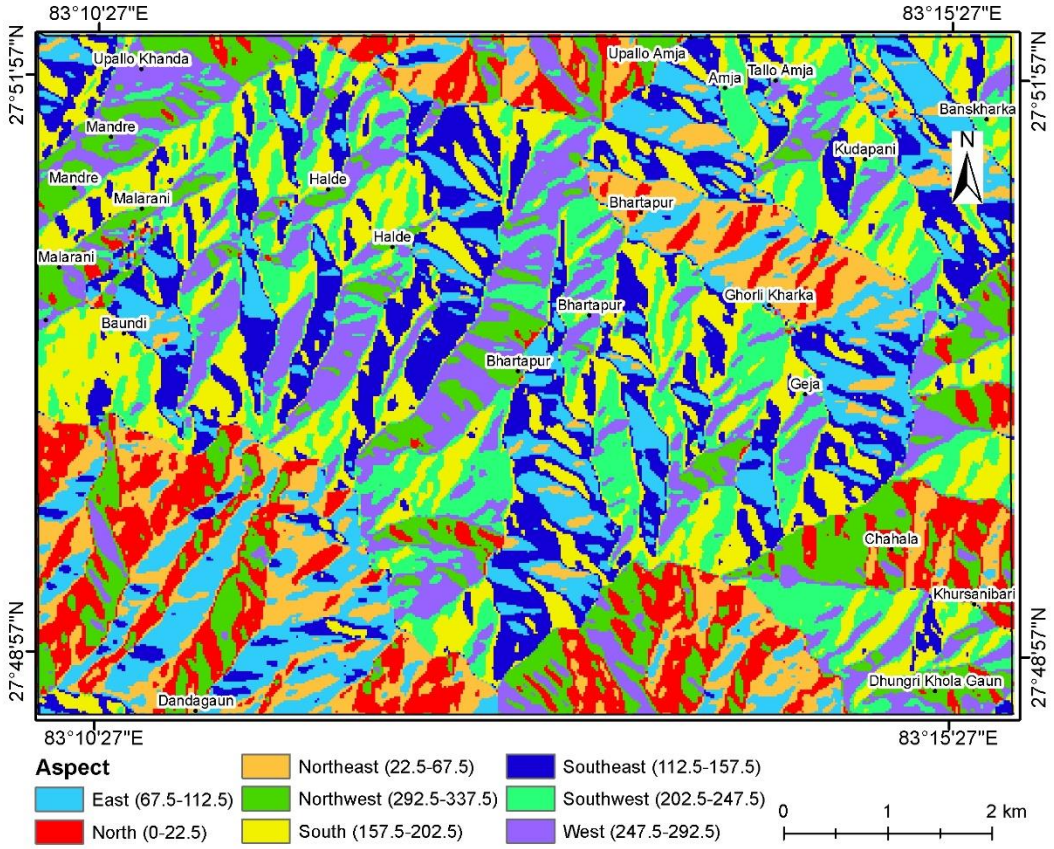

Figure 8 Aspect map of the study area.

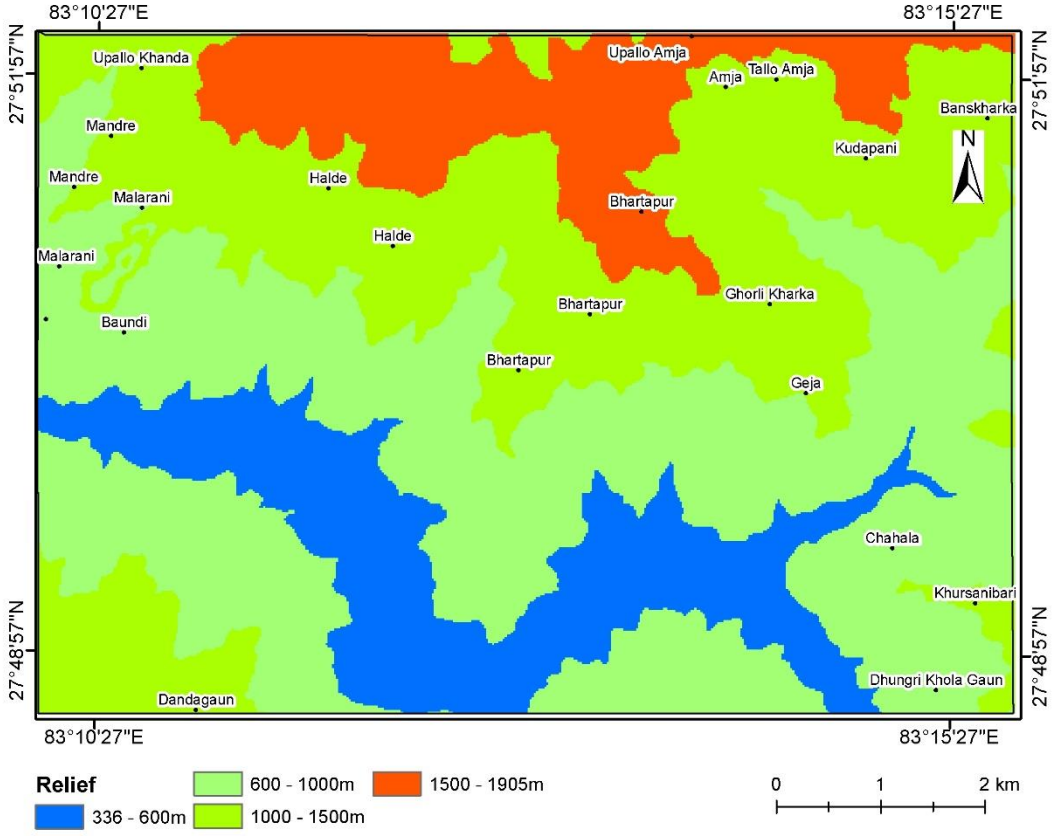

Figure 9 Relief map of the study area.

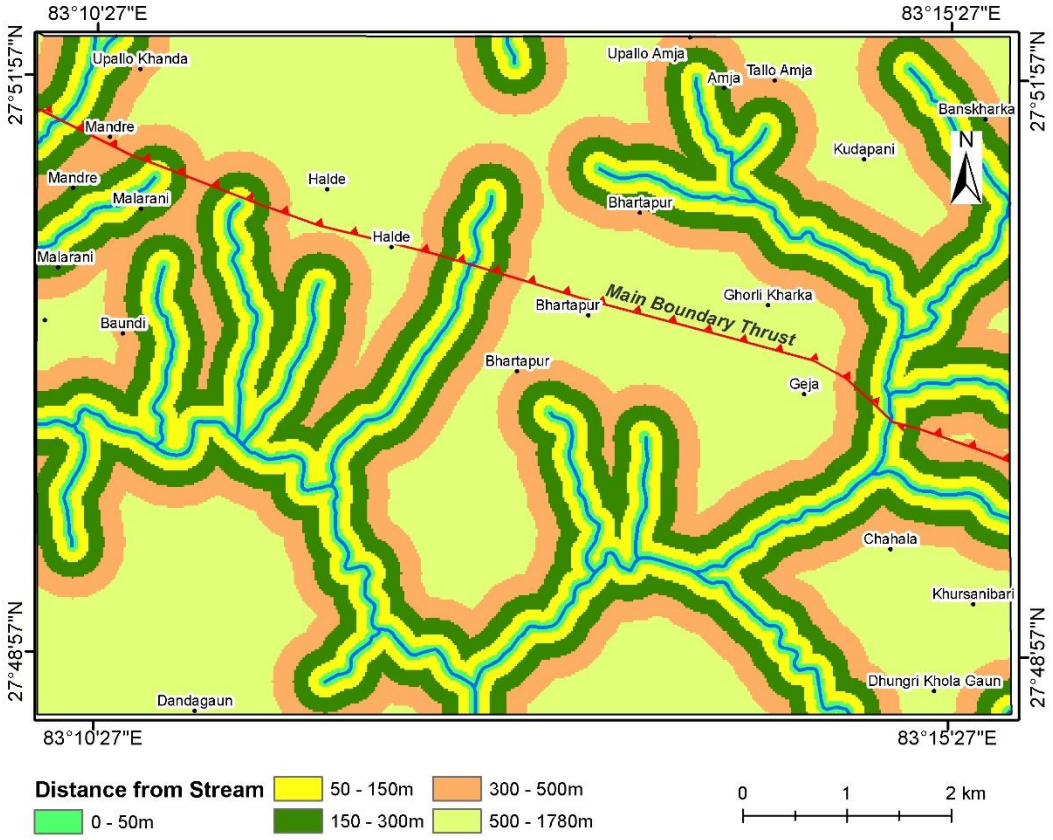

Figure 10 Distance to stream map of the study area.

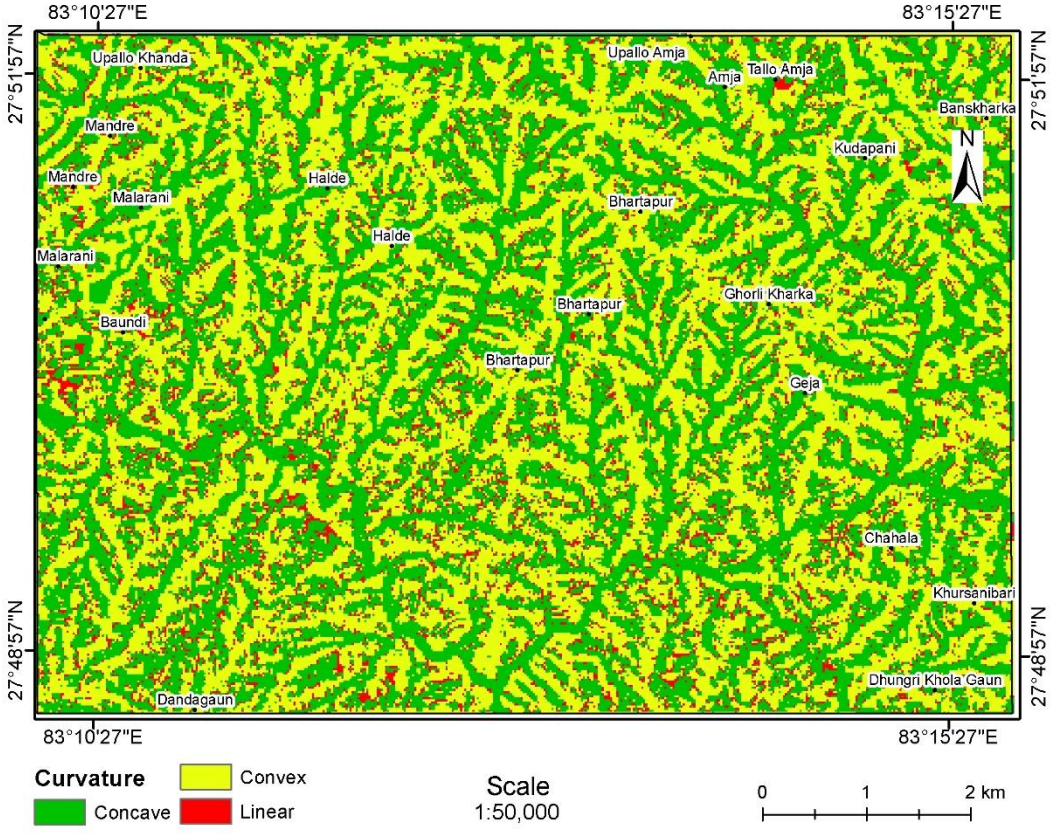

Figure 11 Curvature map of the study area.

Distance from the Road

Utilizing the linear road data of the research region, the distance from the road map (Fig. 12) was created. The Euclidean distance tool, which represents each cell's link to a source or collection of sources based on the straight-line distance, was used to calculate the distance to the road map (Fig. 12). Six categories of distance from the road were created: 0–50 m, 50–150 m, 150–300 m, 300–500 m, 500–1000 m, and 1000–1853 m.

According to Table 1, the area between 0 and 50 meters in height accounts for 10.3% of the total landslide and 12.6% of the entire research area. The region between 150 and 300 meters and 300 and 500 meters from the road has a high frequency ratio of 1.30 and 1.27, and it is also likely to have landslides in the future.

Concave curvature has a higher FR value than concave curvature (1.02), making it more prone to landslides.

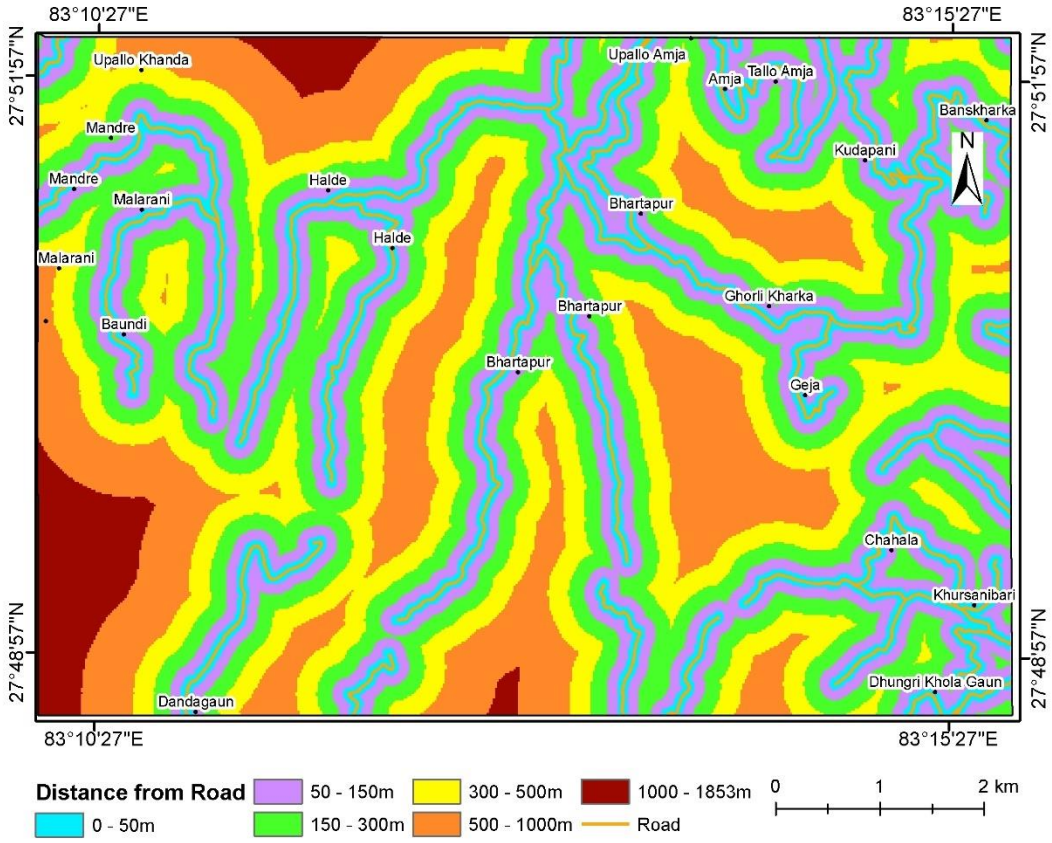

Figure 12 Distance from the road map.

Table 1 Factors with landslide inventory showing area coverage.

Domain	Class	Class Pixel	Area (sq. km)	Class pixel %	Landslide pixel	Area (sq. km)	Landslide pixel %
Slope	0 - 10	5186	2.07	3.37	19	0.0076	3.11
	10 - 20	18789	7.52	12.23	40	0.016	6.56
	20 - 30	45284	18.11	29.46	139	0.0556	22.79
	30 - 40	60982	24.39	39.68	323	0.1292	52.95
	40 - 50	22791	9.12	14.83	86	0.0344	14.10
	50 - 64	658	0.26	0.43	3	0.0012	0.49
Total		**153690**	**61.48**	**100.00**	**610**	**0.244**	**100.00**
Distance to Thrust (MBT)	0 – 500 m	25623	10.25	16.81	247	0.0988	40.49
	500 – 1000 m	24618	9.85	16.15	124	0.0496	20.33
	1000 – 2000 m	44094	17.64	28.92	122	0.0488	20.00
	2000 – 4000 m	50293	20.12	32.99	114	0.0456	18.69
	4000 – 5319 m	7823	3.13	5.13	3	0.0012	0.49
Total		**152451**	**60.98**	**100.00**	**610**	**0.244**	**100.00**
Land-use	Forest	110509	44.20	72.49	300	0.12	49.18
	Agricultural Land	30594	12.24	20.07	11	0.0044	1.80
	Bushes	8465	3.39	5.55	11	0.0044	1.80
	Barren Land	1036	0.41	0.68	259	0.1036	42.46

Domain	Class	Class Pixel	Area (sq. km)	Class pixel %	Landslide pixel	Area (sq. km)	Landslide pixel %
	Sand	1847	0.74	1.21	29	0.0116	4.75
Total		**152451**	**60.98**	**100.00**	**610**	**0.244**	**100.00**
Geology	Middle Siwalik	90768	36.31	59.54	551	0.2204	90.33
	Swat Formation	1243	0.50	0.82	7	0.0028	1.15
	Melpani Formation	4569	1.83	3.00	0	0.000	0.00
	Suntar Formation	1695	0.68	1.11	0	0.000	0.00
	Lower Siwalik	6255	2.50	4.10	3	0.001	0.49
	Khara Formation	10592	4.24	6.95	0	0.000	0.00
	Katuwa Formation	8167	3.27	5.36	10	0.004	1.64
	Aru Formation	17454	6.98	11.45	34	0.014	5.57
	Charchare Formation	7546	3.02	4.95	0	0.000	0.00
	Gawar Formation	4162	1.66	2.73	5	0.002	0.82
Total		**152451**	**60.98**	**100.00**	**610**	**0.244**	**100.00**
Distance to Stream	0 –50 m	12654	5.06	8.30	73	0.029	11.97
	50 –150 m	21393	8.56	14.03	89	0.036	14.59
	150 – 300 m	29812	11.92	19.56	117	0.047	19.18
	300 – 500 m	31695	12.68	20.79	192	0.077	31.48
	500 – 1780 m	56897	22.76	37.32	139	0.056	22.79
Total		**152451**	**60.98**	**100.00**	**610**	**0.244**	**100.00**
Curvature	Concave	68345	27.34	44.47	277	0.111	45.41
	Linear	12436	4.97	8.09	41	0.016	6.72
	Convex	72909	29.16	47.44	292	0.117	47.87
Total		**153690**	**61.48**	**100.00**	**610**	**0.244**	**100.00**
Aspect	North	14707	5.88	9.57	10	0.004	1.64
	Northeast	15246	6.10	9.92	22	0.009	3.61
	East	19683	7.87	12.81	66	0.026	10.82
	Southeast	22359	8.94	14.55	125	0.050	20.49
	South	25821	10.33	16.80	118	0.047	19.34
	Southwest	21215	8.49	13.80	114	0.046	18.69
	West	19244	7.70	12.52	91	0.036	14.92
	Northwest	15415	6.17	10.03	64	0.026	10.49
Total		**153690**	**61.48**	**100.00**	**610**	**0.244**	**100.00**
Relief	336 – 600 m	22295	8.92	14.51	79	0.032	12.95
	600 – 1000 m	63894	25.56	41.57	260	0.104	42.62
	1000 – 1500 m	49448	19.78	32.17	228	0.091	37.38
	1500 – 1905 m	18053	7.22	11.75	43	0.017	7.05
Total		**153690**	**61.48**	**100.00**	**610**	**0.244**	**100.00**
Distance from Road	0 – 50 m	19301	7.72	12.56	63	0.025	10.33
	50 – 150 m	30589	12.24	19.90	135	0.054	22.13
	150 – 300 m	37694	15.08	24.53	195	0.078	31.97
	300 – 500 m	32212	12.88	20.96	163	0.065	26.72
	500 – 1000 m	26957	10.78	17.54	54	0.022	8.85
	1000 – 1853 m	5698	2.28	3.71	0	0.000	0.00
Total		**152451**	**60.98**	**99.19**	**610**	**0.244**	**100.00**

Table 2 Frequency ratio of each class

Domain	Class	Class Pixel	Class pixel %	Landslide pixel	Landslide pixel %	Frequency Ratio (FR)	Relative Frequency (RF)	RF (Non %)	Min RF	Max RF	Max-Min RF	(Max-Min) Min RF	PR
Slope	0 - 10	5186	3.37	19	3.1	0.92	0.16	16.29	0.09	0.24	0.14	0.07	2.12
	10 - 20	18789	12.23	40	6.6	0.54	0.09	9.47					
	20 - 30	45284	29.46	139	22.8	0.77	0.14	13.65					
	30 - 40	60982	39.68	323	53.0	1.33	0.24	23.55					
	40 - 50	22791	14.83	86	14.1	0.95	0.17	16.78					
	50 - 64	658	0.43	3	0.5	1.15	0.20	20.27					
Total		**153690**	**100.0**	**610**	**100.0**	**5.67**	**1.00**	**100.00**					
Distance to Thrust (MBT)	0 – 500 m	25623	16.8	247	40.49	2.41	0.48	47.97	0.02	0.48	0.46		6.92
	500 – 1000 m	24618	16.1	124	20.33	1.26	0.25	25.07					
	1000 – 2000 m	44094	28.9	122	20.00	0.69	0.14	13.77					
	2000 – 4000 m	50293	33.0	114	18.69	0.57	0.11	11.28					
	4000 – 5319 m	7823	5.1	3	0.49	0.10	0.02	1.91					
Total		**152451**	**100.0**	**610**	**100**	**5.02**	**1.00**	**100**					

Domain	Class	Class Pixel	Class pixel %	Landslide pixel	Landslide pixel %	Frequency Ratio (FR)	Relative Frequency (RF)	RF (Non %)	Min RF	Max RF	Max-Min RF	(Max-Min) Min RF	PR
Land use	Forest	110509	72.5	300	49.2	0.68	0.01	1.01	0.00	0.93	0.92		13.88
	Agricultural Land	30594	20.1	11	1.8	0.09	0.001	0.13					
	Bushes	8465	5.6	11	1.8	0.32	0.005	0.48					
	Barren Land	1036	0.7	259	42.5	62.48	0.93	92.57					
	Sand	1847	1.2	29	4.8	3.92	0.06	5.81					
Total		**152451**	**100.0**	**610**	**100**	**67.50**	**1.00**	**100**					
Geology	Middle Siwalik	90768	59.5	551	90.3	1.52	0.37	36.67	0.00	0.37	0.37		5.51
	Swat Formation	1243	0.8	7	1.1	1.41	0.34	34.02					
	Melpani Formation	4569	3.0	0	0.0	0.00	0.00	0.00					
	Suntar Formation	1695	1.1	0	0.0	0.00	0.00	0.00					
	Lower Siwalik	6255	4.1	3	0.5	0.12	0.03	2.90					
	Khara Formation	10592	6.9	0	0.0	0.00	0.00	0.00					
	Katuwa Formation	8167	5.4	10	1.6	0.31	0.07	7.40					
	Aru Formation	17454	11.4	34	5.6	0.49	0.12	11.77					
	Charchare Formation	7546	4.9	0	0.0	0.00	0.00	0.00					
	Gawar Formation	4162	2.7	5	0.8	0.30	0.07	7.26					
Total		**152451**	**100.0**	**610**	**100.0**	**4.14**	**1.00**	**100.00**					
Distance to Stream	0 – 50 m	12654	8.3	73	12.0	1.44	0.26	25.81	0.18	0.27	0.10		1.43
	50 – 150 m	21393	14.0	89	14.6	1.04	0.19	18.61					
	150 – 300 m	29812	19.6	117	19.2	0.98	0.18	17.56					
	300 – 500 m	31695	20.8	192	31.5	1.51	0.27	27.10					
	500 – 1780 m	56897	37.3	139	22.8	0.61	0.11	10.93					
Total		**152451**	**100.0**	**610**	**100**	**5.59**	**1.00**	**100**					
Curvature	Concave	68345	44.5	277	45.4	1.02	0.357	35.69	0.29	0.36	0.07		1.00
	Linear	12436	8.1	41	6.7	0.83	0.290	29.04					
	Convex	72909	47.4	292	47.9	1.01	0.353	35.27					
Total		**153690**	**100.0**	**610**	**100.0**	**2.86**	**1.00**	**100.00**					
Aspect	North	14707	9.6	10	1.64	0.2	0.02	2.27	0.02	0.19	0.16		2.47
	Northeast	15246	9.9	22	3.61	0.4	0.05	4.83					
	East	19683	12.8	66	10.82	0.84	0.11	11.22					
	Southeast	22359	14.5	125	20.49	1.41	0.19	18.70					
	South	25821	16.8	118	19.34	1.15	0.15	15.29					
	Southwest	21215	13.8	114	18.69	1.35	0.18	17.98					
	West	19244	12.5	91	14.92	1.19	0.16	15.82					
	Northwest	15415	10.0	64	10.49	1.0	0.14	13.89					
Total		**153690**	**100.0**	**610**	**100.00**	**8**	**1.00**	**100.00**					
Relief	336 – 600 m	22295	14.5	79	13.0	0.89	0.24	24.26	0.16	0.32	0.15		2.29
	600 – 1000 m	63894	41.6	260	42.6	1.03	0.28	27.86					
	1000 – 1500 m	49448	32.2	228	37.4	1.16	0.32	31.57					
	1500 – 1905 m	18053	11.7	43	7.0	0.60	0.16	16.31					
Total		**153690**	**100.0**	**610**	**100.0**	**3.68**	**1.00**	**100.00**					
Distance from Road	0 – 50 m	19301	12.6	63	10.3	0.82	0.16	16.39	0.10	0.26	0.16		2.39
	50 – 150 m	30589	19.9	135	22.1	1.11	0.22	22.16					
	150 – 300 m	37694	24.5	195	32.0	1.30	0.26	25.98					
	300 – 500 m	32212	21.0	163	26.7	1.27	0.25	25.41					
	500 – 1000 m	26957	17.5	54	8.9	0.50	0.10	10.06					
	1000 – 1853 m	5698	3.7	0	0.0	0.00	0.00	0.00					
Total		**152451**	**99.2**	**610**	**100**	**5.02**	**1.00**	**100**					

Landslide Susceptibility Analysis

By integrating all nine-factor maps, a Landslide Susceptibility Index (LSI) map was created (Fig. 13(a)). Final LSI = $PR_{d1}*FR_1 + PR_{d2}*FR_2 + PR_{d3}*FR_3 + PR_{d4}*FR_4 + \ldots\ldots\ldots + PR_{dn}*FR_n$

Where,
PR = Predictive ratio of each factor
FR = Frequency ratio of each class of a factor (Influencing domain)

Here, the domain or influencing factor from Table 1 is given weight in the predictive ratio (Acharya & Lee, 2019) (Table 3), which is determined as shown in eq. 3 below:

PR = (Maximum RF – Minimum RF)/ (Minimum RF of Maximum RF – Minimum RF) - - - Eq. 3.

RF is an abbreviation for relative frequency. It is the proportion of a domain's class FR to the domain's overall FR.

Table 3 Weight of individual domain or factors.

Factor / Domain	PR	Weight
Curvature	1.00	100
Distance to stream	1.43	143
Slope gradient	2.12	212
Relief / Elevation	2.29	229
Distance to Road	2.39	239
Aspect	2.47	247
Geology	5.51	551
Distance to Thrust	6.92	692
Land use	13.88	1388

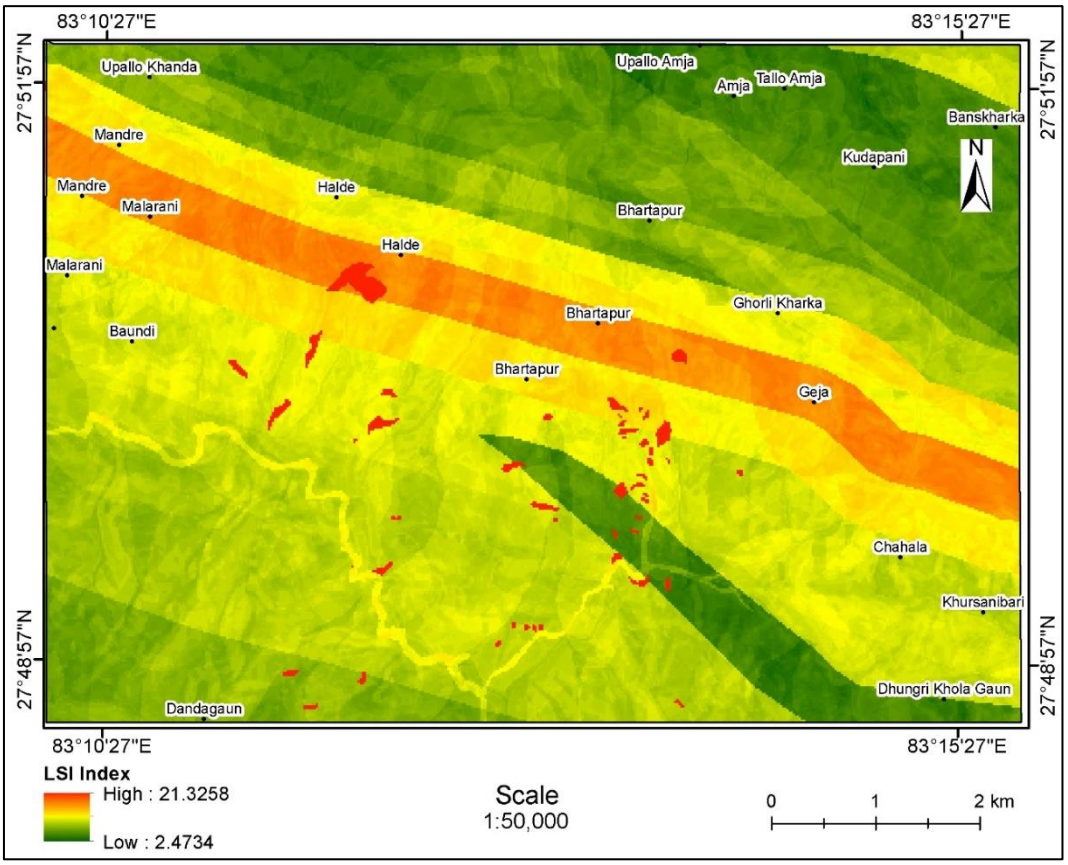

Figure 13(a) Landslide Susceptibility Index (LSI) map.

Equation (2) was used to produce LSI. The ROC/AUC curve was used to categorize LSI data. IBM-SPSS Statistics 20's success rate curves were used to conduct a qualitative analysis of the LSI (landslide susceptibility index) in order to assess the predicting ability of the suggested frequency technique for the landslide potential zone. The area under the success rate curve (ROC/AUC) in the aforementioned plot Fig. 13(b) is 0.796, suggesting that the analysis is accurate, and that the prediction rate was 82.2% with an upper bound of 84.2%. The success rate for determining landslide potential shows that 20% of the study area has a high rank and might account for 68% of the area's total landslides. Additionally, 40% and 50% of the proposed GWP levels might each account for around 85% and 90% of all known landslides. A final map of landslide susceptibility is created utilizing the three Groundwater Potential classifications that have been established: stable zone (more than 40%), quasi-stable zone (20-40%), and unstable zone (0-20%). In order to create the final landslide susceptibility maps (Fig. 14), the LSI was divided into three susceptibility zones, namely the stable zone, quasi-stable zone, and unstable zone, with threshold values of corresponding classes of 4.08, 4.65, and 15.72, respectively (Table 4).

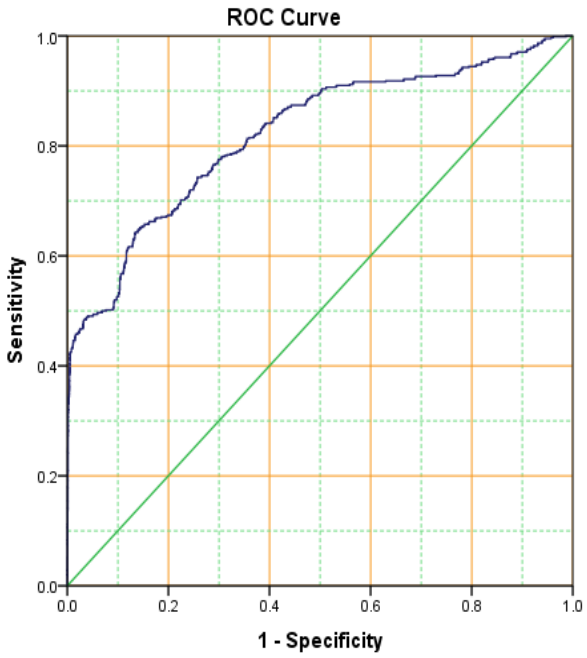

Case Summary	
Slide	Valid N (listwise)
Positive	610
Negative	152447

Larger values of the test result variable(s) indica stronger evidence for a positive actual state.

a. The positive actual state is 1.

Area Under the Curve

Test Result Variable(s): LSI

Area	Std. Error	Asymptotic Sign	Asymptotic 95% Confidence Interval	
			Lower Bound	Upper Bound
.822	.010	.000	.802	.842

The test result variable(s): LSI has at least one t between the positive actual state group and th negative actual state group. Statistics may be biase

a. Under the nonparametric assumption

b. Null hypothesis: true area = 0.5

Figure 13(b) ROC/AUC Curve of the LSI model.

Table 4 Upper boundary value set for different landslide susceptibility classes.

Cumulative %	**Class Name**	**LSI**
		Upper Bound
60%	Stable Zone	5.4837
80%	Quasi Stable Zone	6.2129
100%	Unstable Zone	21.3258

Table 5 Areal coverage by different landslide susceptibility classes.

Landslide Susceptibility				**Method of Classification**
LSI Class	**Pixel Count**	**Area (sq. km)**	**Area %**	
Stable	91216	36.49	59.83%	**ROC/AUC Curve**
Quasi Stable	30641	12.26	20.10%	
Unstable	30590	12.24	20.07%	
Total	**152447**	**60.98**	**100%**	

The final susceptibility map (Fig. 14), which was created using 9 influencing factor maps, indicates that the villages of Geja, Bhartapur, Halde, Malarani, and Mandre are in an unstable zone and are prone to flooding. The quasi-stable zone includes Baundi, Halde, Malarani, and Ghorli Kharka. The rest of the settlements are in a stable zone. Out of the total study area, 59.83 percent is stable (Banskharka, Kudapani, Tallo Amja, Amja, Upallo Amja, Bhaetapur, Upallo Khanda, Dandagaun, Chahala, Khursanibari, and Dhungri Khola Gaun), 20.1 percent is quasi stable, and 20.07 percent is unstable and very prone to landslides in the near future (Fig. 15; Table 5).

Landslide Causative Factors

The contributing factors in this study were chosen based on the literature reviews, existence or absence and the significance of the attributing factors for landslides. The geomorphological, anthropogenic, and extrinsic components were all included in the landslide conditioning factors. In this study, the distance from thrust (MBT), aspect, slope, land use/land cover, relief, distance from stream, geology, distance from road, and curvature were taken into account while preparing the landslide susceptibility map. Table 1 provides the allocated weights for each type of causative factor.

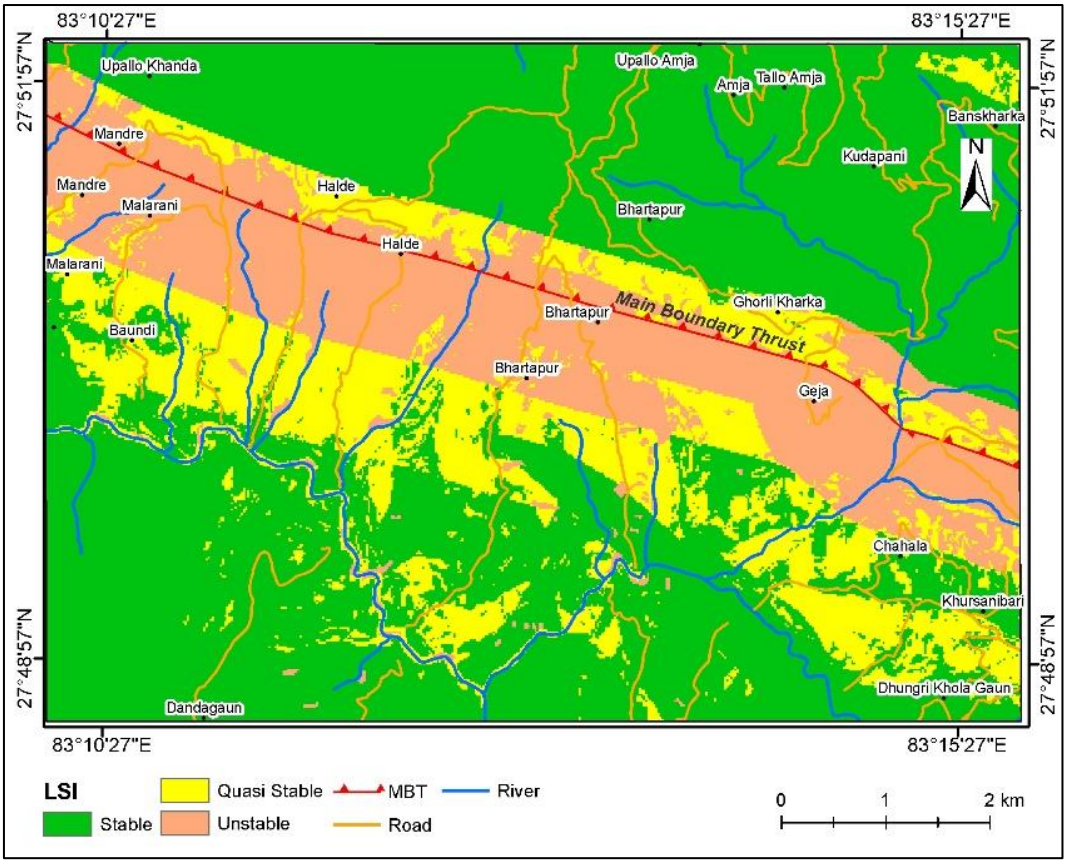

Figure 14. Landslide susceptibility map of the study area.

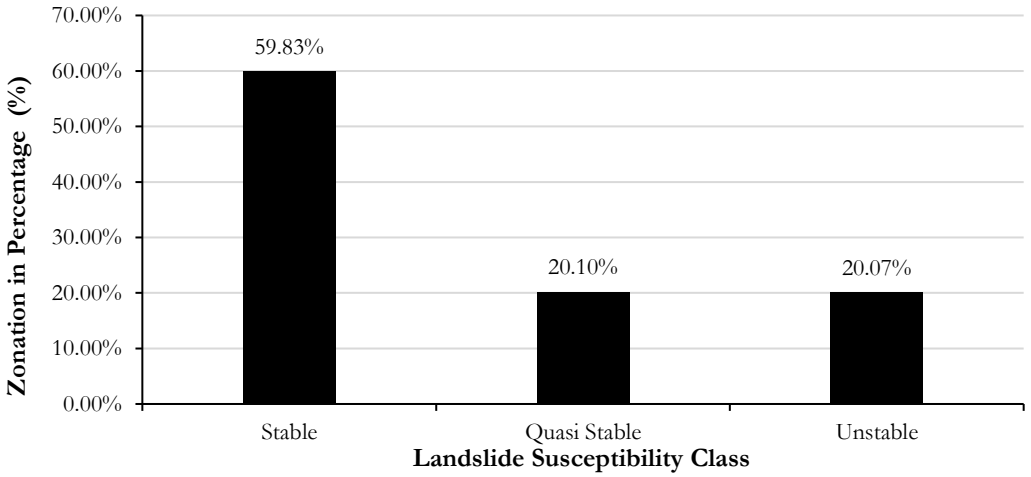

Figure 15. Final landslide susceptibility class in Mandre-Khursanibari.

The Mandre-Khursanibari region is prone to several slope instability difficulties because of the high slope, rough landscape, and weak rock state. The frequency ratio method's deduced weights demonstrate that the terrain slope significantly affects the distribution of landslides. In general, as the gradient of the terrain increases, landslides occur more frequently. The majority of the landslides in our research area, however, accumulated between 30 and 40 degrees, giving the area a high-frequency ratio of 1.33 and making it the most prone to landslides. (Table 1).

The southeast, southwest, and west facing aspects have the greatest frequency ratio values, according to the aspect map's frequency ratio (Table 1). The greatest FR is 1.41 on the southeast aspect, followed by 1.35 on the southwest and 1.19 on the west slope (Table 1). The high-frequency ratios are 1.44 and 1.51 at the distances of 0 to 50 meters and 300 to 500 meters from the streams, respectively. The barren terrain has the greatest FR of all the land uses, at 62.48. According to Table 1, it was discovered that the research area's

concave curvature surface is more prone to landslides because convex curvature has a high frequency of landslide occurrence with a FR value of 1.02. Additionally, it was noted that the Middle Siwalik zone, which has a FR value of 1.52, followed by the Swat Formation and Aru Formation, with FR values of 1.41 and 0.49 respectively, was where most of the landslides occurred. Both the role of lithology and the presence of regional thrust can be considered as the major cause for landslide in several regions.

Distance from the road implies that areas 0–50 m and 300–500 m are more prone to landslides, due to their higher FR values of 1.44 and 1.51 respectively. The zone between 0 and 500 m distance is most prone to landslides since it is the distance closest to the thrust, where MBT has the highest frequency ratio value of 2.41.

Topographic Parameters

In the analysis of earthquake-induced landslides, the digital elevation model (DEM) has been a key component (Kamp et al., 2008; Wang et al., 2015). Although there is no clear correlation between height and the likelihood of a landslide occurring, research indicates that the possibility increases with elevation (Ercanoglu et al., 2004). The elevation range between 600 m and 1500 m has the highest landslide concentration. Another important topographic feature that is included in landslide susceptibility research is the slope's steepness (Wang et al., 2015; Kamp et al., 2008; Regmi et al., 2016; Regmi et al., 2010; Pradhan & Lee 2010). Fig. 7 illustrates the slope's range, which is 0° to 64°. The slope range between 30° and 40° has the highest landslide concentration. The slope's aspect mimics moisture retention and its relationship to the rock formation's bedding pattern, which in turn impacts the material's physical characteristics and susceptibility to failure (Dai et al., 2001). According to this study, landslides are mostly caused by aspects to the west, southwest, and southeast (Fig. 8). It often occurs because several landslides occur on the slope towards the river and the majority of the river segment trends towards SW-SE.

Given its significant impact in causing slope instability, the slope's surface undulation can have a significant impact on the occurrence of landslides. Landslides typically occur on convex slopes and concave slopes along curves (Neupane & Paudyal, 2021) (Fig. 11). Landslides brought on by earthquakes frequently occur on convex slopes (Reneau & Dietrich, 1987). When building roads, the area between 150 and 300 meters from the road is more prone to landslides.

Anthropogenic Factors

One of the landslide conditioning elements is land use, as changes in land use may affect the plant cover and thus affect mechanical and hydrological aspects (e.g., soil strength and slope behavior; see, for example, Greenway, 1987; van Westen et al., 2003; Reichenbach et al., 2014). The variance in the distribution of land uses may be either natural, caused by humans, or both. The frequency ratio weight values show that there is a larger association between barren land (62.48) and other land use groups, and our conclusion is consistent with that value.

Conclusions

In the present study, the Frequency Ratio model was used as a statistical approach to assess the geographical likelihood of landslides. Each factor layer was weighted, revealing positive correlations between the model's predictions and field circumstances, this verifies the FR method's ability to forecast the likelihood of landslides occurrence. Among the 72 landslides studied, a notable 40% were found to be strongly influenced by the proximity to the thrust (MBT). Notably, the Middle Siwalik zone emerged as a hotspot for landslides, as identified by the geology factor map. The lithological setting especially the hard rocks resting over the soft rocks like mudstone, shale and claystone are the prime cause for landslides in many cases. A significant finding lies in the identification of slope angles between 30^0 and 40^0 as prime areas for landslide occurrences, emphasizing the role of steeper slopes and increased relief. Moreover, the terrain map analysis predicted that the number of landslides would fall when 1000 meters elevation is exceeded. In the Mandre-Khursanibari region, the present study reshapes the understanding of landslide susceptibility. While agricultural and forested areas dominate the landscape, the results imply that barren terrain is more susceptible to landslides. Importantly, the study underscores the direct association between the distance from the thrust and landslide occurrences, with the highest distribution of landslides within 0 to 500 meters distance from the MBT zone. The presence of the MBT in this region has made the rocks inherently weak. The rocks in the MBT zone are highly crushed, sheared and intensely fractured. The major cause of the landslide is ultimately connected with the active tectonics of this MBT in the region. The most important aspect of our findings lies in the identification of factors viz. distance from the thrust and geology as primary contributors to landslide initiation in the Mandre-Khursanibari area. This insight not only enhances our understanding of local susceptibility but also holds implications for proactive land-use planning and targeted mitigation strategies. As we advance our understanding of landslide dynamics, future research could explore innovative methodologies and technologies to refine predictive models, ultimately contributing to more effective risk management practices in landslide-prone regions.

Acknowledgements: Authors are grateful to the Central Department of Geology for providing the equipment for field investigation. Our heartfelt appreciation goes to Ravi Nepal, Pramod Kattel, and Pradip Shrestha for their dedication and assistance during the fieldwork.

Author Contributions: The first author spearheaded

the research project's planning and execution, conducting extensive fieldwork and geological data collection. Additionally, the first author took the lead in interpreting the findings and spearheading the discussions. The second author played a pivotal role in generating thematic maps through GIS analysis, ensuring accurate representation of spatial data. Both authors collaborated closely in refining the manuscript incorporating the suggestions and comments from the reviewers.

Conflict of Interests: The authors declare no conflict of interest.

Data Availability Statement: The data that support the finding of this study are available from the corresponding author, upon reasonable request.

References

Acharya, M., Dhakal, R.P., & Paudyal, K R. (2023). Application of frequency ratio method for landslide susceptibility mapping at the Thulo Lumpek area, Gulmi, Nepal. *Journal of Development Innovations*, 7(2), 56-76.

Acharya, T.D., & Lee, D.H. (2019). Landslide susceptibility mapping using relative frequency and predictor rate along Araniko Highway. *KSCE Journal of Civil Engineering*, 23(2), 763-776.

Althuwaynee O.F., Pradhan B., & Lee S. (2016). A novel integrated model for assessing landslide susceptibility mapping using CHAID and AHP pair-wise comparison. International *Journal of Remote Sensing*, 37(5), 1190-1209.

Aghdam I.N., Varzandeh M.H.M., & Pradhan B. (2016). Landslide susceptibility mapping using an ensemble statistical index (Wi) and adaptive neuro-fuzzy inference system (ANFIS) model at Alborz Mountains (Iran). *Environmental Earth Sciences*, 75(7), 553.

Bonham-Carter, G.F. (1994). *Geographic information systems for geoscientists.* PERGAMON PRESS, Modeling with GIS, OXFORD.

Budha, P.B., Paudyal, K.R., & Ghimire, M. (2016). Landslide susceptibility mapping in eastern hills of Rara Lake, western Nepal. *Journal of Nepal Geological Society*, 50(1), 125-131.

Camarinha P.I.M., Canavesi V., & Alval´a, R.C.S. (2014). Shallow landslide prediction and analysis with risk assessment using a spatial model in a coastal region in the state of Sao Paulo, Brazil. *Natural Hazards and Earth System Sciences*, 14(9), 2449-2468.

Chen, W., Chai, H., Sun, X., Wang, Q., Ding, X., & Hong, H. (2016a). A GIS-based comparative study of frequency ratio, statistical index and weights-of-evidence models in landslide susceptibility mapping. *Arabian Journal of Geosciences*, 9 (3), 204.

Chen, W., Wang, J., Xie, X., Hong, H., Van Trung, N., Bui, D.T., Wang, G., & Li, X. (2016b). Spatial prediction of landslide susceptibility using integrated frequency ratio with entropy and support vector machines by different kernel functions. *Environmental Earth Sciences,* 75 (20), 1344.

Chen, W., Xie, X., & Wang, J. (2017). A comparative study of the logistic model tree, random forest, and classification and regression tree models for spatial prediction of landslide susceptibility. *Catena*, 151, 147–160.

Conforti, M., Pascale. S., Robustelli. G., & Sdao. F. (2014). Evaluation of prediction capability of the artificial neural networks for mapping landslide susceptibility in the Turbolo River catchment (northern Calabria, Italy). *Catena*, 113, 236–250.

Dahal, A., & Paudyal, K.R. (2022). Mapping of geological sensitive areas along the Budhi Khola watershed, Sunsari/Morang districts, eastern Nepal Himalaya. *Karma Quest International*, 6(1), 44-68.

Dai, F.C., Lee, C.F., Li.J., Xu, & Z.W. (2001). Assessment of landslide susceptibility on the natural terrain of Lantau Island, Hongkong. *Environmental Geology*, 40(3), 381–391.

Ding, Q., Chen, W., & Hong, H., (2017). Application of frequency ratio, weights of evidence and evidential belief function models in landslide susceptibility mapping. *Geocarto International*, 32(6), 619–639.

Ercanoglu, M., Gokceoglu, C., & Van Asch, T.W. (2004). Landslide susceptibility zoning north of Yenice (NW Turkey) by multivariate statistical techniques. *Natural Hazards*, 32(1), 1–23.

Fayez, L., Pham, B.T., Solanki, H.A., Pazhman, D., Dholakia, M.B., Khalid, M., & Prakash, I. (2018). Application of frequency ratio model for the development of landslide susceptibility mapping at part of Uttarakhand State, India. *International Journal of Applied Engineering Research*, 13(9), 6846-6854.

Feizizadeh, B., Shadman, M., Roodposhti, M.S., Jankowski, P., & Blaschke, T. (2014). A GIS-based extended fuzzy multi-criteria evaluation for landslide susceptibility mapping. *Computers and Geosciences*, 73, 208–221.

Ghimire, M. (2011). Landslide occurrence and its relation with terrain factors in the Siwalik Hills, Nepal: case study of susceptibility assessment in three basins. *Natural Hazards*, *56*(1), 299–320.

Greenway, D.R. (1987). Vegetation and slope stability. In: Anderson, M.G., Richards, K.S (Eds.), *Slope Stability*, pp. 187–230.

Goetz, J.N., Brenning, A., Petschko, H., & Leopold, P. (2015). Evaluating machine learning and statistical prediction techniques for landslide susceptibility modeling. *Computers and Geosciences*, 81, 1–11.

Hong, H., Pourghasemi, H.R., & Pourtaghi, Z.S. (2016). Landslide susceptibility assessment in Lianhua County (China): a comparison between a random forest data mining technique and bivariate and multivariate statistical models. *Geomorphology*, 259, 105–118.

Kannan, M., Saranathan, E., & Anabalagan, R. (2013). Landslide vulnerability mapping using frequency ratio model: a geospatial approach in Bodi-Bodimettu Ghat section, Theni district, Tamil Nadu, India. *Arabian Journal of Geosciences*, 6(8), 2901–2913.

Kamp, U., Growley, B.J., Khattak, G.A., & Owen, L.A., (2008). GIS-based landslide susceptibility mapping for the 2005 Kashmir earthquake region.

Geomorphology, 101(4), 631–642.

K.C., J., Gautam, D., Neupane, P., & Paudyal, K.R. (2018). Landslide inventory mapping and assessment along the Ramche-Jharlang area in Dhading, Rasuwa, and Nuwakot districts, Lesser Himalaya, central Nepal. *Journal of Nepal Geological Society*, 55, 103-108.

Lee, S., Hong, S., & Jung, H. (2017). A support vector machine for landslide susceptibility mapping in Gangwon province, Korea. *Sustainability*, 9(1), 48.

Lee, S., & Park, I. (2013). Application of decision tree model for the ground subsidence hazard mapping near abandoned underground coal mines. *Journal of Environmental Management*, 127, 166–176.

Lee, M.-J., Park, I., & Lee, S. (2015). Forecasting and validation of landslide susceptibility using an integration of frequency ratio and neuro-fuzzy models: a case study of Seorak mountain area in Korea. *Environmental Earth Sciences*, 74(1), 413– 429.

Lee, S., & Talib, J.A. (2005). Probabilistic landslide susceptibility and factor effect analysis. *Environmental Geology*, 47(7), 982–990.

Mondal, S., & Maiti, R. (2013). Integrating the analytical hierarchy process (AHP) and the frequency ratio (FR) model in landslide susceptibility mapping of Shiv-khola watershed. *International Journal of Disaster Risk Science*, 4(4), 200–212.

Montgomery, D.R., & Dietrich, W.E. (1994). A physically based model for the topographic control on shallow land sliding. *Water Resources Research*, 30(4), 1153–1171.

Neupane, A., & Paudyal, K.R. (2021). Lithological Control on Landslide in the Siwalik Section of the Lakhandehi Khola Watershed of Sarlahi District, South-Eastern Nepal. *Journal of Development Innovations*, 5(2), 44-65.

Neupane, A., Paudyal, K.R., Devkota, K.C., & Dhungana, P. (2023). Landslide susceptibility analysis using frequency ratio and weight of evidence approaches along the Lakhandehi Khola watershed in the Sarlahi District, southern Nepal. *Geographical Journal of Nepal*, 16(01), 73–96.

Park, I., Lee, J., & Saro, L. (2014). Ensemble of ground subsidence hazard maps using fuzzy logic. *Central European Journal of Geosciences*, 6(2), 207–218.

Paudyal, K.R., & Maharjan, R. (2022). Landslide susceptibility mapping of the Main Boundary Thrust (MBT) region in Tinau-Mathagadhi Section of Palpa District, Lumbini Province. *Journal of Nepal Geological Society*, 63(01), 99–108.

Peng, L., Niu, R.Q., Huang, B., Wu, X.L., Zhao, Y.N., & Ye, R.Q. (2014). Landslide susceptibility mapping based on rough set theory and support vector machines: a case of the Three Gorges area, China. *Geomorphology*, 204, 287–301.

Pham, B.T., Tien, B.D., Dholakia, M.B., Prakash, I., & Pham, H.V. (2016). A comparative study of least square support vector machines and multiclass alternating decision trees for spatial prediction of rainfall-induced landslides in a tropical cyclones area. *Geotechnical and Geological Engineering*, 34(6), 1807-1824.

Pradhan, B. (2011). Manifestation of an advanced fuzzy logic model coupled with Geo-information techniques to landslide susceptibility mapping and their comparison with logistic regression modeling. *Environmental and Ecological Statistics*, 18(3), 471–493.

Pradhan, B. (2013). A comparative study on the predictive ability of the decision tree, support vector machine and neuro-fuzzy models in landslide susceptibility mapping using GIS. *Computers and Geosciences*, 51, 350–365.

Pradhan, B., & Lee, S. (2010). Landslide susceptibility assessment and factor effect analysis: backpropagation artificial neural networks and their comparison with frequency ratio and bivariate logistic regression modeling. *Environmental Modelling and Software*, 25(6), 747–759.

Pradhan, B. (2013). Landslide susceptibility mapping of a catchment area using frequency ratio, fuzzy logic, and multivariate logistic regression approaches. *Journal of the Indian Society of Remote Sensing*, 38(2), 301-320.

Regmi, A.D., Dhital, M.R., Zhang, J.Q., Su, L.J., & Chen, X.Q. (2016). Landslide susceptibility assessment of the region affected by the 25 April 2015 Gorkha earthquake of Nepal. *Journal of Mountain Science,* 13(11), 1941–1957.

Regmi, N.R., Giardino, J.R., & Vitek, J.D. (2010). Modeling susceptibility to landslides using the weight of evidence approach: Western Colorado, USA; *Geomorphology*, 115, 172–187.

Reneau, S.L., & Dietrich, W.E. (1987). Size and location of colluvial landslides in a steep forested landscape. *IAHSAISH*, 165, 39 –48.

Reichenbach, P., Busca, C., Mondini, A.C., & Rossi, M. (2014). The influence of land use change on Landslide Susceptibility Zonation: The Briga Catchment Test Site (Messina Italy), *Environmental Management*, 54(6), 1372–1384.

Reis, S., Yalcin, A., Atasoy, M., Nisanci, R., Bayrak, T., Erduran, M., Sancar, C., & Ekercin, S. (2012). Remote sensing and GIS-based landslide susceptibility mapping using frequency ratio and analytical hierarchy methods in Rize province (NE Turkey). *Environmental Earth Sciences*, 66(7), 2063-2073.

Steger, S., Brenning, A., Bell, R., Petschko, H., & Glad,e T. (2016). Exploring discrepancies between quantitative validation results and the geomorphic plausibility of statistical landslide susceptibility maps. *Geomorphology*, 262, 8–23.

Taylor, M.J., & Burns, S.F. (2005). *Slope and seismic stability of Castel Lake Debris Dam*. St. Helens, Washington.

Tien, B.D., Tuan, T.A., & Hoang, N.D. (2017). Spatial prediction of rainfall-induced landslides for the Lao Cai area (Vietnam) using a hybrid intelligent approach of least squares support vector machines inference model and artificial bee colony optimization. *Landslides*, 14(2), 447–458.

Tsangaratos, P., & Benardos, A. (2014). Estimating landslide susceptibility through a artificial neural network classifier. *Natural Hazards*, 74(3), 1489-1516.

Tsangaratos, P., & Ilia, I. (2016). Landslide susceptibility

mapping using a modified decision tree classifier in the Xanthi Perfection, Greece. *Landslides*, 13(2), 305-320.

Umar, Z., Pradhan, B., Ahmad, A., Jebur, M.N., & Tehrany, M.S. (2014). Earthquake induced landslide susceptibility mapping using an integrated ensemble frequency ratio and logistic regression models in West Sumatera Province, Indonesia. *Catena*, 118, 124–135.

Upreti, B. (2001). *The physiography and geology of Nepal and landslide hazards. Landslide problem mitigation to the Hindukush-Himalayas*. International Centre for Integrated Mountain Development.

Upreti, B.N., & Dhital, M.R. (1996). *Landslide Studies and Management in Nepal*. International Centre for Integrated Mountain Development.

Van Westen, C.J., Rengers, N., & Soeters, R. (2003). Use of geomorphological information in indirect landslide susceptibility assessment. *Natural Hazards*, 30, 399–411.

Wang, L.J., Guo, M., Sawada, K., Lin, J., & Zhang, J. (2015). Landslide susceptibility mapping in Mizunami City, Japan: A comparison between logistic regression, bivariate statistical analysis and multivariate adaptive regression spline models. *Catena*, 135, 271–282.

Wang, Q., & Li, W. (2017). A GIS-based comparative evaluation of analytical hierarchy process and frequency ratio models for landslide susceptibility mapping. *Physical Geography*, 38(4), 318–337.

Wu, Y., Li, W., Wang, Q., Liu, Q., Yang, D., Xing, M., Pei, Y., & Yan, S. (2016). Landslide susceptibility assessment using frequency ratio, statistical index and certainty factor models for the Gangu County, China. *Arabian Journal of Geosciences,* 9(2), 1–16.

Yalcin, A., Reis, S., Aydinoglu, A.C., & Yomralioglu, T. (2011). A GIS based comparative study of frequency ratio, analytical hierarchy process, bivariate statistics and logistics regression methods for landslide susceptibility mapping in Trabzon, NE Turkey. *Catena*, 85(3), 274–287.

Yilmaz, I. (2009). Landslide susceptibility mapping using frequency ratio, logistic regression, artificial neural networks, and their comparison: A case study from Kat landslides (Tokat—Turkey). *Computers & Geosciences*, 35(6), 1125–1138.